The Astrophysical Journal, 893:86 (3pp), 2020 April 10 https://doi.org/10.3847/1538-4357/ab84ea

Erratum: "A Multimass Velocity Dispersion Model of 47 Tucanae Indicates No Evidence for an Intermediate-mass Black Hole" (2019, ApJ, 875, 1)

Christopher R. Mann[1], Harvey Richer[1], Jeremy Heyl[1], Jay Anderson[2], Jason Kalirai[2], Ilaria Caiazzo[1], Swantje D. Möhle[1], Alan Knee[1], and Holger Baumgardt[3]
[1] Department of Physics and Astronomy, University of British Columbia, Vancouver, BC V6T 1Z1, Canada
[2] Space Telescope Science Institute, 3700 San Martin Drive, Baltimore, MD 21218, USA
[3] School of Mathematics and Physics, University of Queensland, St. Lucia, QLD 4068, Australia
Received 2020 March 23; published 2020 April 17

A simple, but non-trivial error has been discovered in the analysis of Mann et al. (2019). The nature of the error was a multiplicative factor in the portion of the analysis code that converts between the dimensionless units used for internal calculations and the physically meaningful units (i.e., solar masses and arcseconds) displayed as results. The erroneous factor was related to the size of the distribution in question (i.e., its a parameter). The overall effect was that the stellar remnant and binary population masses, being more tightly distributed, were being disproportionately inflated.

We also note an unrelated typo in Table 2, where the reported binary fractions (f) were too small by a factor of 10, has also been identified and corrected. In this case, the error was merely typographic and had no effect on the results.

The analysis has been re-run with a corrected unit conversion process. The affected Tables 2 and 3 and Figures 5–8 have been recreated and are presented here with their original numberings. The figures and tables have been reproduced with the same retention fraction (8.5%) of stellar-mass black holes (sBHs) and neutron stars (NSs) as was used in the initial publication in order to facilitate comparison. However, this value no longer holds particular significance.

Our results are affected as follows. Overall, the concentrated populations of binaries and stellar remnants do not contribute as strongly to the central velocity dispersion as previously determined. The trend between the fitted intermediate-mass black hole (IMBH) mass and the choice of the retention fraction is qualitatively similar, but the strength is much diminished. Thus, the constraint we placed on the sBH and NS retention of $\lesssim$8.5% in the original publication must be relaxed. Additionally, the results of Kızıltan et al. (2017) ($M_{\rm IMBH}/M_{\rm Cl} = 0.3\%$) are now consistent with a retention fraction of ∼25% by the new analysis. The predicted IMBH mass does not drop to zero until the retention fraction approaches 100%, indicating the sBH population cannot fully account for the central velocity dispersion rise unless one can justify a nearly total retention of the inferred population.

The parameter values reported at the beginning of the original Section 4.1 for a 8.5% retention model should be replaced with: $M_{\rm IMBH} = 4400 \pm 1900\,M_\odot$, $M_{\rm Cl} = (1.177 \pm 0.017) \times 10^6\,M_\odot$, $a_{\rm Cl} = 41\farcs1 \pm 1\farcs2$, and an $M_{\rm IMBH}/M_{\rm Cl}$ ratio of 0.37% ± 0.16%.

Table 2
Model Inputs for Binaries and Stellar Remnants

Object Type	Subgroup Parameters/Type	Primary Mass (M_p) Range ($M_\odot$)	$\langle M_p \rangle$ ($M_\odot$)	Object Mass ($M_\odot$)	Retention Fraction	Population Mass ($M_\odot$)	a ($''$)
Binaries	q = [0.5, 0.7]	0.80–0.86	0.83	1.33	1	5987	18.61
	($\langle q \rangle = 0.60$)	0.74–0.80	0.77	1.23	1	5510	20.07
	($f = 0.0265$)	0.67–0.74	0.71	1.13	1	5040	21.72
		0.61–0.67	0.64	1.03	1	4307	23.71
		0.55–0.61	0.58	0.93	1	4224	26.12
	q = [0.7, 0.9]	0.80–0.86	0.83	1.50	1	2381	16.64
	($\langle q \rangle = 0.80$)	0.74–0.80	0.77	1.38	1	2185	17.95
	($f = 0.0098$)	0.67–0.74	0.71	1.27	1	1992	19.42
		0.61–0.67	0.64	1.16	1	1696	21.20
		0.55–0.61	0.58	1.05	1	1656	23.36
	q = [0.9, 1.0]	0.80–0.86	0.83	1.62	1	1006	15.42
	($\langle q \rangle = 0.95$)	0.74–0.80	0.77	1.50	1	922	16.63
	($f = 0.0039$)	0.67–0.74	0.71	1.38	1	839	18.00
		0.61–0.67	0.64	1.26	1	713	19.65
		0.55–0.61	0.58	1.13	1	694	21.65
Remnants	WD	⋯	⋯	1.2	1	24000	20.52
	NS	⋯	⋯	1.4	0.085	23800	17.72
	sBH	⋯	⋯	10	0.085	19000	2.74

Note. With corrected conversion factor and typo in f values. The object mass within a binary subgroup is calculated as $\langle M \rangle (1 - \langle q \rangle)$. There is a total mass of ∼39,000 $M_\odot$ in binaries and ∼27,600 $M_\odot$ in stellar remnants (taking into account the 8.5% retention of NSs and sBHs). Population masses for binaries are calculated as described in Equation (7). Population masses for stellar remnants are calculated by assuming an object mass, determining the distribution parameter (a) from that mass, and then consulting the predicted progenitor counts of Figure 3 that have been corrected to include the entire cluster instead of the limited field of view. Population mass values presented are before retention is considered.

Table 3
Exploring Retention Fraction

Retention (%)	$M_{\rm IMBH}$ ($M_\odot$)	$M_{\rm Cl}$ ($M_\odot$)	$a_{\rm Cl}$ ($''$)	$\frac{M_{\rm IMBH}}{M_{\rm Cl}}$	ln L
0.0	4710	1178830	40.89	0.0040	−310215.245
8.5	4377	1176723	41.07	0.0037	−310215.090
12.5	4221	1175736	41.15	0.0036	−310215.017
25.0	3733	1172671	41.42	0.0032	−310214.796
37.5	3244	1169638	41.69	0.0028	−310214.581
50.0	2756	1166636	41.97	0.0024	−310214.374
62.5	2268	1163668	42.25	0.0019	−310214.173
75.0	1781	1160733	42.54	0.0015	−310213.980
87.5	1294	1157834	42.84	0.0011	−310213.795
100.0	808	1154973	43.14	0.0007	−310213.619

Note. With a corrected conversion factor. Enforcing various retention fractions for NSs and sBHs provides different fit results. Typical uncertainties for these parameters are very similar to those reported at the end of this work for the 8.5% retention case. Interpolating these values shows retention of ∼31% is required to obtain the Kızıltan et al. (2017) mass fraction of 0.30%. The fitted IMBH mass does not become negligible until the retention fraction becomes approaches 100%. Corresponding velocity dispersion profiles are shown in Figure 8.

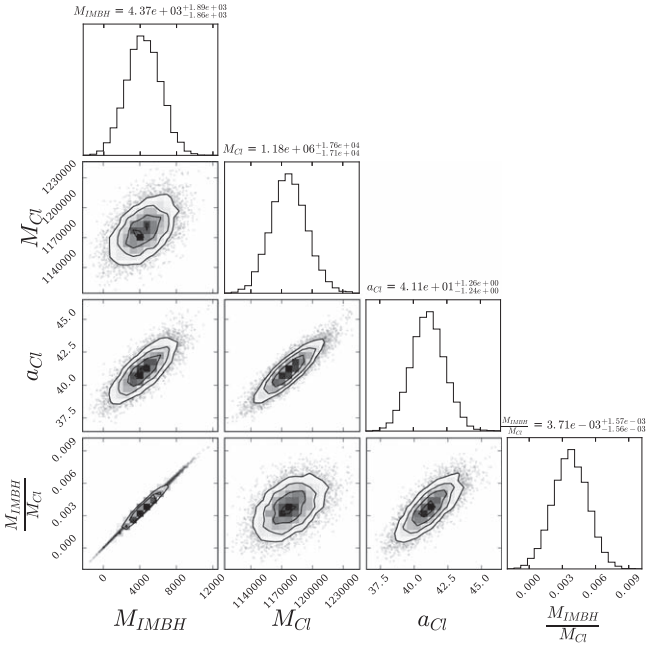

Figure 5. With a corrected conversion factor. Results from bootstrapping the proper motion data and fitting the velocity dispersion model. The bootstrap method (randomly drawing stellar data points with replacement for each iteration) provides a spread of fit parameters around the best-fitting values that give a measure of the uncertainty in each parameter.

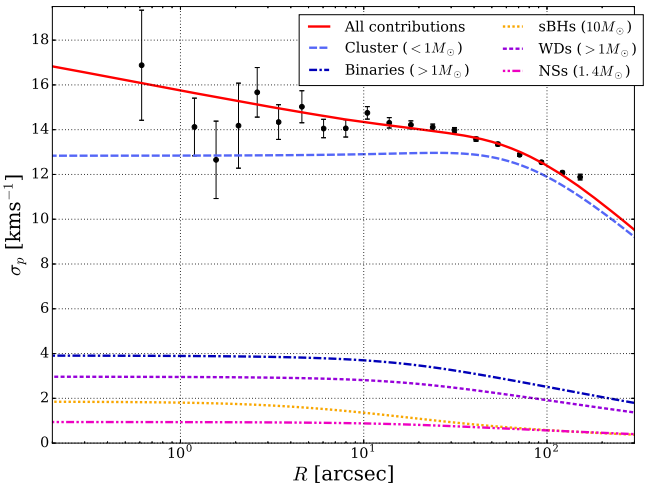

Figure 6. With a corrected conversion factor. The solid red line shows the best-fitting (unbinned) velocity dispersion model. It includes the IMBH, binary, remnant, and low-mass cluster object components. Model parameters are given in Table 2. Note that the black points display binned data and are included for visualization purposes only. The model was fit using an unbinned likelihood maximization. Dashed lines show how the different components (cluster stars, binaries, sBHs, WDs, and NSs) contribute to the overall velocity dispersion profile with the individual components being added in quadrature.

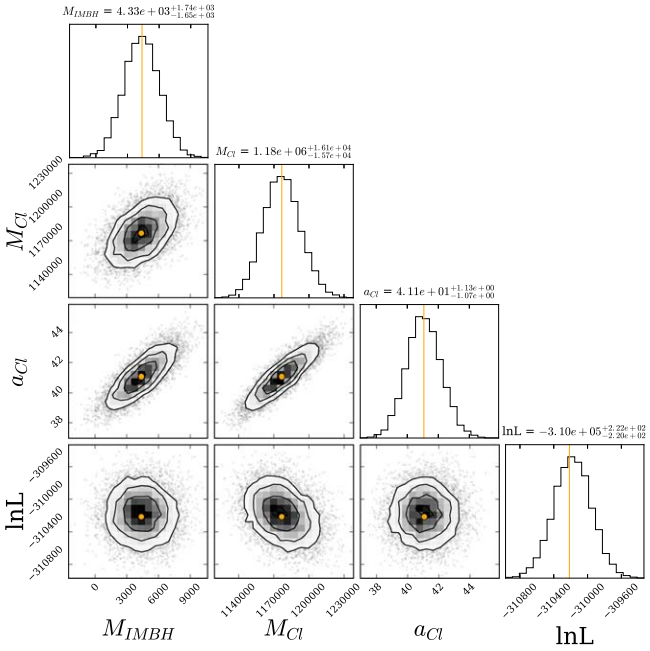

Figure 7. With a corrected conversion factor. Presented here are the fit results of the artificially sampled data sets. The artificial velocities are drawn from the original data's best-fit velocity dispersion model. All fits used unbinned likelihood maximization. The orange dots and vertical lines indicate the fit values of the original data. There are two major conclusions to be drawn from this exercise: (1) the proximity of each orange line to the mean of the $M_{\rm IMBH}$, $M_{\rm Cl}$, and $a_{\rm Cl}$ distributions indicates no systematic bias in our model's ability to recover input parameters; and (2) the proximity of the original data's $\ln L$ value to the mean of the artificial distribution shows our model is indeed a good fit to the shape of the velocity data.

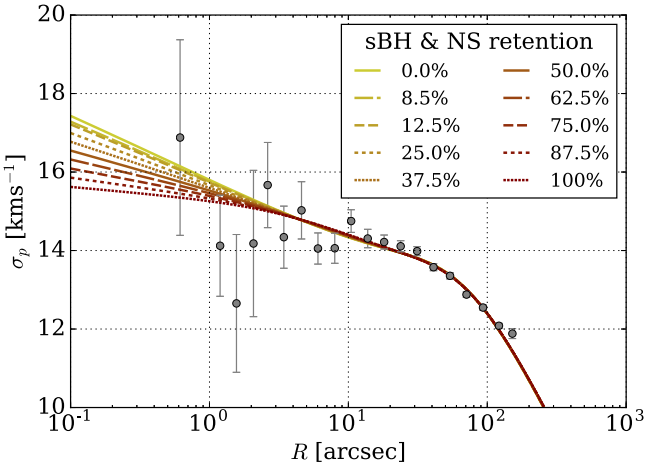

Figure 8. With a corrected conversion factor. Velocity dispersion profiles corresponding to the different NS and sBH retention fractions explored in Table 3. The overall log-likelihood difference between these models is small due to the relatively few data points at low radius where the models differ most substantially (see Table 3).

We would like to thank Sebastian Hoof for his diligence in verifying our results and his aid in locating the cause of the disparity.

ORCID iDs

Christopher R. Mann https://orcid.org/0000-0002-9312-0073

References

Kızıltan, B., Baumgardt, H., & Loeb, A. 2017, Natur, 542, 203
Mann, C. R., Richer, H., Heyl, J., et al. 2019, ApJ, 875, 1